THE JOURNAL OF PHYSICAL CHEMISTRY B

Article

pubs.acs.org/JPCB

Isotopic Preferential Solvation of I^- in Low-Temperature Water Nanoclusters

Pablo E. Videla,[†] Peter J. Rossky,[‡] and Daniel Laria*[,†,§]

[†]Departamento de Química Inorgánica Analítica y Química-Física e INQUIMAE, Facultad de Ciencias Exactas y Naturales, Universidad de Buenos Aires, Ciudad Universitaria, Pabellón II, 1428 Buenos Aires, Argentina

[‡]Department of Chemistry, Rice University, Houston, Texas 77005-1892, United States

[§]Departamento de Física de la Materia Condensada, Comisión Nacional de Energía Atómica, Avenida Libertador 8250, 1429 Buenos Aires, Argentina

ABSTRACT: We present results from ring polymer molecular dynamics experiments that provide microscopic insights into the characteristics of the isotopic stabilizations of H and D aqueous species in the first solvation shell of a halide I^- ion in water nanoclusters at low temperatures. The analysis of the simplest $I^-\cdot(HOD)$ dimer shows a clear propensity for the light isotope to lie at the non-hydrogen-bonded dangling position. Our results predict that, at $T \sim 50$ K, $I^-\cdot(DOH)$ isomers are three times more abundant than $I^-\cdot(HOD)$ ones. The reasons for such stabilization can be traced back to differences in the nuclear kinetic energy projected along directions perpendicular to the plane of the water molecule. Dynamical implications of these imbalances are shown to be reflected in the characteristics of the corresponding bands of the infrared spectroscopic signals. A similar analysis performed in larger aggregates containing ~20 water molecules reveals, in contrast, a stabilization of the light isotope along $I^-\cdots HO$ hydrogen bonds. Effects derived from the consideration of smaller halide anions with larger electric fields at the surface are also examined.

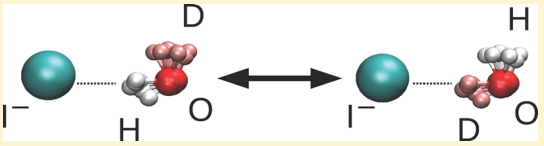

I. INTRODUCTION

Physical interpretations of the characteristics of the solvation of ionic species in aqueous media normally focus on the interplay between ion−water and water−water interactions, which exhibit competitive characteristics. In this context, the analysis of the hydration of simple ions in nanoclusters is enlightening because this analysis can be posed in terms of piecewise modifications that take place in the global arrangement of increasing numbers of solvent molecules around ionic species. Trimers of the type $X^-\cdot(H_2O)_2$ are the simplest aggregates in which the latter competitive ingredients are present. The examination of the sequence X = I, Br, Cl, Fl as the solute species is particularly instructive, revealing the evolution in solvent structure, as one considers anions with increasing water affinity. A large body of spectroscopic[1−4] and theoretical studies[5−14] have clearly demonstrated that, along that sequence, a gradual transition takes place from stable C_1 conformers (characterized by two anionic hydrogen bonds (HB) and a third intrawater one) toward C_2 arrangements, in which the third interaction appears severely weakened or practically missing.

The possibility of incorporating different isotopic species represents an interesting tool to disentangle experimental spectroscopic signals.[15,16] In particular, the consideration of mixed nanoclusters combining H_2O, D_2O, and HOD molecules provides clear signatures of the local solvation structures that prevail in different cluster environments. Using combined path integral molecular dynamics (PIMD) techniques, we recently examined the relative stability of H and D isotopes at dangling (i.e., surface) positions in contrast to connective (i.e., intermolecular) positions in nanoscopic water aggregates.[17] Our analysis showed a clear propensity of light isotopes to lie at the cluster surfaces. Moreover, the characteristics of the predicted infrared spectra reflect this distribution.

The presence of solute species within water clusters introduces additional inhomogeneities in their close vicinities that should naturally lead to differences in the relative isotopic stabilities at connective positions in their closest solvation shells. Using Ar-tagging techniques, Diken et al.[18] have reported mid-infrared spectra of $I^-\cdot(H_2O)$, $I^-\cdot(D_2O)$, and $I^-\cdot(HOD)$; by comparing the magnitudes of different spectral peaks, they concluded that, at temperatures of the order of ~30−40 K, $I^-\cdot(DOH)$ isomers should be 1 order of magnitude more abundant than their $I^-\cdot(HOD)$ counterparts. A follow-up article by Harvath et al.[19] included a much more comprehensive analysis of anharmonicities and isotopic effects on infrared signals from similar dimers, including I^-, Br^-, and Cl^- as solute species. From a theoretical perspective, these studies represent optimal benchmarks to test the performance of Hamiltonians of increasing complexity, such as, for example, the six-dimensional potential energy surface designed by Bowman and collaborators to model interactions in the $Cl^-\cdot(H_2O)$ dimer.[20−22]

Herein, we will present results from ring polymer molecular dynamics[23] (RPMD) simulations that focus on the thermodynamic stability of aqueous H and D atoms in the solvation of a single I^- anion embedded in alternative water clusters. In doing

Received: June 10, 2015
Revised: August 12, 2015

DOI: 10.1021/acs.jpcb.5b05561
J. Phys. Chem. B XXXX, XXX, XXX−XXX

so, we refrain here from implementing highly refined, computationally intensive force fields; instead, we adopted a much simpler, mean-field model Hamiltonian that was specifically designed to correctly capture nuclear quantum effects on the structure and dynamics of bulk water at ambient conditions. Our simulation results show that this level of approximation is not only sufficient to obtain general agreement with direct spectroscopic signals but, equally important, also provides physically sound guidance about key elements that control the differences in the isotopic stabilities and qualitative trends as one considers smaller solutes or varying numbers of solvent molecules.

The organization of this paper is as follows: in section II, we briefly describe the model and methodological details. Section III contains the main results of the study. In section IV, we provide a summary of the main conclusions.

II. MODEL AND SIMULATION PROCEDURE

We examined equilibrium and dynamical characteristics of aqueous nanoclusters combining HOD and H_2O and containing, in addition, a single X^- anion [$X^- = I^-$ or Br^-]. The propensity of each isotope to coordinate with the solute was analyzed by performing computer simulations relying on the RPMD scheme developed by Manolopoulos et al.[23] to describe nuclear quantum effects. For equilibrium properties, predictions from the latter approach can be made effectively exact and coincide with those obtained via standard PIMD sampling.[24] The RPMD method,[23] based on a discretized path-integral approach, provides approximate quantum nuclear dynamics, as well.

As we mentioned in the previous section, our force field is the q-TIP4P/F model[25] that has been tailored to properly mimic quantum nuclear effects on the structure and dynamics of bulk water. We should mention that this Hamiltonian incorporates nonharmonic intramolecular interactions, a key element to properly capturing effects derived from isotopic substitutions.[26] In a similar spirit, solute−solvent interactions were taken from the best-fits reported in ref 27 for the related, four-site, rigid TIP4P model, without further modification, assuming the usual geometric and arithmetic means for combining length and energy parameters, respectively. As a direct test to validate the use of this model for the present purpose of exploring isotope effects on ion solvation, we computed the solute−oxygen radial distribution function for bulk water at ambient conditions. The profile (not shown) presents a main maximum located at $r = 3.60$ Å, followed by a first minimum at $r = 4.15$; moreover, the area under this main peak includes an average number of nearest water neighbors of ∼7.2. These set of values agree reasonably with previous simulation studies performed with nonpolarizable[27−29] and polarizable[30,31] potential models as well as a more recent ab initio simulation.[32]

RPMD trajectories were generated by implementing a transformation from Cartesian to normal-mode coordinates.[33] In addition, we incorporated a multiple-time-step algorithm[34] that discriminated fast components (i.e., intramolecular interactions in the isomorphic polymers and intramolecular contributions to V) from the rest of the (more slowly varying) components of the forces. Appropriate canonical sampling was obtained by coupling each normal mode to a chain of three Nosé−Hoover thermostats.[35] Time-dependent information was collected from ensembles of 50 microcanonical, not thermostated, runs lasting typically ∼100 ps, with statistically independent, initial configurations taken from previous canonical trajectories. In all cases, the number of discrete path integral points needed is rather large and was set to $P = 300$. With this P value, averages obtained from statistically independent experiments performed at $T = 50$ K presented differences that were below 2%.

III. RESULTS

Before embarking on the analysis of isotopic stability, we present information about the quality of the predictions of our simulations employing the model Hamiltonian mentioned in the previous section. In Table 1, we list a set of relevant equilibrium distances and angles corresponding to global minimum configurations for $X^-\cdot(H_2O)$ ($X^- = I^-$ or Br^-) dimers using the q-TIP4P/F Hamiltonian, along with results obtained from quantum calculations reported in refs 13 and 19. The overall geometry of these configurations is similar to the one depicted in Figure 1a; one observes a connective H_c along an anionic HB and a second H_d at a dangling position. In what follows, subscripts "c" and "d" will denote these connectivities, respectively. The direct examination of the data shows that differences in the interatomic distances do not surpass ∼2%. Note that in some cases, these differences are comparable to computational uncertainties. The largest discrepancies appear in the alignment of the ionic HB, somewhat less marked in the q-TIP4P/F case, which is reflected in the magnitudes of ϕ_{OH_bX}. Still, for both solutes, the differences are, at most, ∼ 8−9%. As such, this level of agreement justifies our model treatment of the interactions for the purpose of examining trends semi-quantitatively.

Table 1. Equilibrium Geometries for $X^-\cdot(H_2O)$

parameter	Br^-	I^-
r_{OH_d}	0.94	0.94
	0.96[a]	0.96[a]
r_{OH_c}	0.97	0.96
	0.99[a]	0.98[a]
	0.98[b]	0.97[b]
r_{XH_c}	2.37	2.66
	2.29[a]	2.55[a]
	2.38[b]	2.75[b]
$\phi_{H_dOH_c}$	100.3	100.7
	100.6[a]	100.6[a]
	99.7[b]	99.4[a]
ϕ_{OH_cX}	158.0	152.3
	167.5[a]	165.4[a]
$\chi_{H_dOH_cX}$	180.0	180.0
	180.0[a]	180.0[a]

[a]From ref 19. [b]From ref 13. Lengths are given in angstroms; angles ϕ and χ are expressed in degrees. Subscripts "c" and "d" refer to connective and dangling positions.

III.A. The $I^-\cdot$(DOH) dimer. We will start by examining the propensities of the two isotopes to lie at dangling and connective positions in the $I^-\cdot$(HOD) dimer. The interconversion process of interest can be described in terms of the following reaction:

$$I^-\cdot(H_cOD_d) \rightarrow I^-\cdot(D_cOH_d) \quad (1)$$

DOI: 10.1021/acs.jpcb.5b05561
J. Phys. Chem. B XXXX, XXX, XXX−XXX

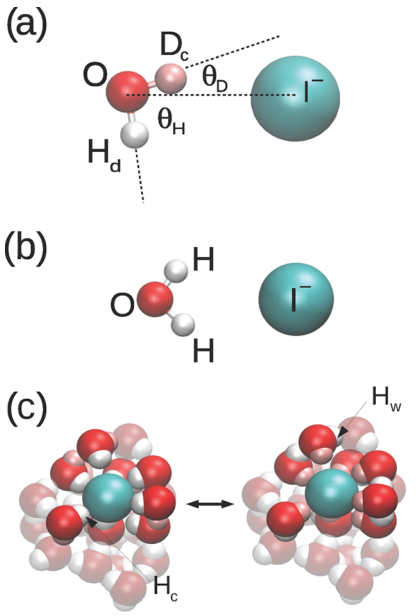

Figure 1. (a) Snapshot of an $I^-\cdot(HOD)$ dimer configuration in the vicinity of the free-energy global minimum, $\xi \sim 60°$ (see text). (b) C_{2v} transition-state configuration for the interchange between connecting and dangling hydrogens in $I^-\cdot(H_2O)$. (c) H ↔ D interchange shown in eq 11. For clarity, D atoms are rendered in pink.

The relative stabilities of reactant and product states in the previous equation can be computed from the associated free-energy profile, namely:

$$\beta A(\xi^+) \propto \langle \delta(\xi - \xi^+) \rangle \tag{2}$$

where ξ represents an order parameter that clearly discriminates between reactive and product states. In the present context, we found it convenient to adopt the following definition:

$$\xi = \theta_H - \theta_D \tag{3}$$

where

$$\cos\theta_i = \frac{r_{OI}^{cnt} \cdot r_{Oi}^{cnt}}{|r_{OI}^{cnt}||r_{Oi}^{cnt}|} \tag{4}$$

In the previous equation, $r_{ij}^{cnt} = r_j^{cnt} - r_i^{cnt}$ and

$$r_i^{cnt} = \frac{1}{P}\sum_{k=1}^{P} r_i^{(k)} \tag{5}$$

represents the centroid coordinate of the ith water nucleus (see Figure 1a). Clearly, negative (positive) values of ζ correspond to $I^-\cdot(H_cOD_d)$ ($I^-\cdot(D_cOH_d)$) configurations.

In Figure 2, we present the profile for $\beta A(\zeta)$ for the H ↔ D interchange (black circles) at T = 50 K. The results were obtained by implementing a standard umbrella sampling procedure.[36] The sampling was controlled by adding to the original Hamiltonian an extra-bias harmonic term, $V_{bias}(\zeta)$, of the type:

$$V_{bias}(\xi) = \frac{k_{bias}}{2}(\xi - \xi_0)^2 \tag{6}$$

with $k_{bias} \sim 3 \times 10^{-4}$ kcal/(mol deg^{-2}). A total of five overlapping windows, centered at equidistant values of ξ_0, were necessary to span the $[-75°, 75°]$ interval of the order

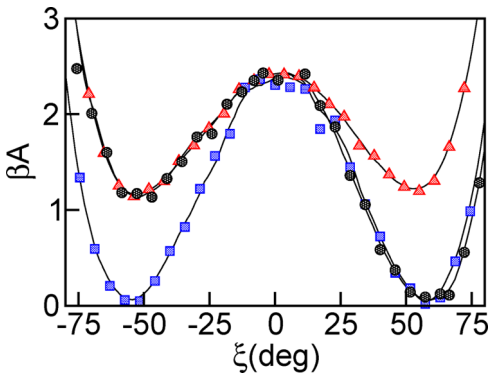

Figure 2. Free-energy profile for the reaction shown in eq 1 (black circles) at T = 50 K. Also shown are results for the interchange between connecting and dangling hydrogen atoms in $I^-\cdot(H_2O)$ (red triangles) and deuterium atoms in $I^-\cdot(D_2O)$ (blue squares).

parameter. The plot of $A(\xi)$ presents a global minimum close to $\xi \sim 60°$, which confirms the stability of the conformer exhibiting a free H; on the other hand, the maximum of the curve that corresponds to the transition-state lies practically at ξ = 0. The free-energy difference between stable states is of the order of 1.2 $k_BT \sim 40$ cm^{-1}, a value that agrees reasonably well with the estimate reported from differences between zero-point energy (ZPE) obtained from experimental mid-infrared signals and theoretical data, $\Delta V_{ZPE} \sim 56$ cm^{-1}.[18]

For the sake of completeness, in Figure 2 we have also included symmetric profiles for the interchange between bonding and dangling positions of hydrogen atoms in H_2O (red triangles) and the deuterium atoms in D_2O (blue squares). These translocations involve the passage over the C_{2v} transition-state structure depicted in Figure 1b. Note that the magnitudes of the free-energy barriers computed from the stable reactant and product states of eq 1 remain reasonable estimates for the corresponding barriers of the profiles for H_2O and D_2O. More importantly, the ~1.15 k_BT reduction in the magnitude of the activation barrier in the H_2O case, compared to the one for D_2O, demonstrates the important modifications due to the different magnitudes of ZPE and tunneling effects in light and heavy water.

In ref 18, it was suggested that the H stabilization at the dangling position was controlled by the magnitude of the frequency of the out-of-plane (OOP) intermolecular vibration, which corresponds to frustrated rotations of the water molecule. In what follows, we will present additional evidence that supports this observation. Our analysis will start by considering the harmonic approximation for ΔA proposed by Ceriotti et al.,[37] namely:

$$\Delta A \sim 2[1 - (m_H/m_D)^{1/2}](\langle T_{H_d}\rangle - \langle T_{H_c}\rangle) \tag{7}$$

In the previous expression, $\langle T_{H_i}\rangle$ represents the average quantum kinetic energy of the light isotope at position i (i = d,c). Within the context of a path-integral scheme, the values of $\langle T_{H_i}\rangle$ can be computed from the following virial estimate:[38]

$$\langle T_{H_i}\rangle = \frac{3}{2\beta} + \left\langle \frac{1}{2P}\sum_{j=1}^{P}(r_{H_i}^{(j)} - r_{H_i}^{cnt})\cdot\nabla_{r_{H_i}^{(j)}}V \right\rangle \tag{8}$$

In Table 2a, we present results for $\langle T_{H_i}\rangle$ and $\langle T_{D_i}\rangle$in the $I^-\cdot(HOD)$ dimer. One observes that the coulomb coupling with

DOI: 10.1021/acs.jpcb.5b05561
J. Phys. Chem. B XXXX, XXX, XXX−XXX

Table 2. Average Kinetic Energy (meV) for H and D Atoms in Aqueous Clusters Containing I^- at Different Connective Positions

	$I^-\cdot(HOD)$		
	H_d	H_c	$H_d - H_c$
$\langle T_{H_i}\rangle$	139.1	149.8	−10.7
$\langle T^{\parallel}_{H_i}\rangle$	99.9	98.5	1.4
$\langle T^{IP}_{H_i}\rangle$	27.2	31.7	−4.5
$\langle T^{OOP}_{H_i}\rangle$	11.9	19.5	−7.6
	D_d	D_c	$D_d - D_c$
$\langle T_{D_i}\rangle$	94.2	101.0	−6.8
$\langle T^{\parallel}_{D_i}\rangle$	72.2	68.9	3.3
$\langle T^{IP}_{D_i}\rangle$	15.5	18.9	−3.4
$\langle T^{OOP}_{D_i}\rangle$	6.5	13.2	−6.7
	$I^-\cdot(HOD)_n[H_2O]_{21-n}$ [a]		
	H_w	H_c	$H_w - H_c$
$\langle T_{H_i}\rangle/n$	153.2	151.1	2.1
$\langle T^{\parallel}_{H_i}\rangle/n$	98.6	99.8	−1.2
$\langle T^{IP}_{H_i}\rangle/n$	33.2	32.2	1.0
$\langle T^{OOP}_{H_i}\rangle/n$	21.4	19.1	2.3
	D_w	D_c	$D_w - D_c$
$\langle T_{D_i}\rangle/n$	105.2	103.6	1.6
$\langle T^{\parallel}_{D_i}\rangle/n$	69.2	70.2	−1.0
$\langle T^{IP}_{D_i}\rangle/n$	21.2	20.4	0.8
$\langle T^{OOP}_{D_i}\rangle/n$	14.8	13.0	1.8

[a]Here, n refers to the number of water molecules in the halide ion first-solvation shell (see text).

the I^- promotes a net increment of ~11 (~7) meV in the total kinetic energy of the connecting H(D), compared to the dangling one that, according to eq 7, leads naturally rroto the stabilization of the latter geometry. Similar effects were reported in our previous analysis of interconversions between dangling and hydrogen-bond donor hydrogens in $(H_2O)_8$.[17]

We remark that the latter variations in the kinetic energies go hand-in-hand with the extent of the spatial localizations of the corresponding atoms. Consequently, the resulting magnitudes are the result of a complex interplay between the topologies of the intramolecular and intermolecular potential energy surfaces. Following previous analysis,[26,39] we found it useful to decompose the proton kinetic energies into projected contributions along three relevant orthogonal orientations: (i) the first one, hereafter referred to as $\langle T_i^{\parallel}\rangle$, corresponds to the direction parallel to the relevant $\mathbf{r}^{cnt}_{OH}$ vector; (ii) the second one, $\langle T^{IP}\rangle$, corresponds to the in-plane (IP) direction perpendicular to OH vector; and finally, (iii) the third corresponds to $\langle T^{OOP}\rangle$, the OOP direction perpendicular to the plane of the water molecule.

At both the "c" and "d" positions, the quantum increment of the average kinetic energy with respect to the classical result, i.e $0.5\beta^{-1} \sim 2.15$ meV, is clearly dominated by intramolecular interactions. At connecting positions, ionic Coulomb attractions promote a mild softening of the OH_c stretching potential which leads to a small (~1%) depletion of the corresponding kinetic energy. The difference between $\langle T^{IP}_{H_i}\rangle$ reduces the parallel trend, but it is still the difference between the OOP contributions that dominates the overall stabilization of the light isotope at the dangling position (see entries in the fourth column). Inserting the global kinetic energy difference for H atoms into eq 7, one obtains $\beta\Delta A \sim -1.4$, a value that compares favorably with the prediction obtained from the non-Boltzmann sampling mentioned above.

The previous considerations have implications in the time domain which are clearly manifested in the characteristics of the infrared spectra. In Figure 3 we present results for the relative

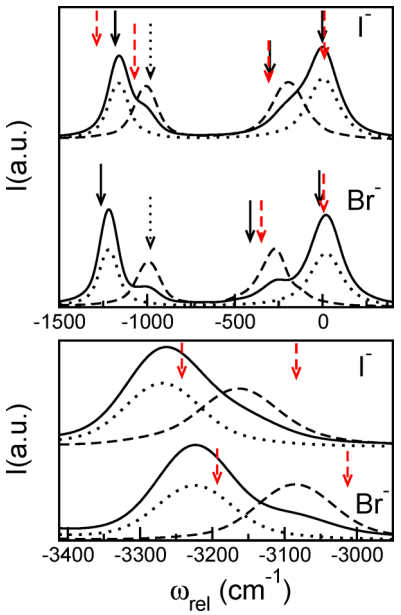

Figure 3. Top panel: calculated relative frequencies of the stretching bands for $X^-\cdot(HDO)$. Shown are results from eq 9: solid lines; $X^-\cdot(H_cOD_d)$ conformer: dashed lines; $X^-\cdot(D_cOH_d)$ conformer: dotted lines. The solid black arrows represent experimental data reported in ref 19. Red dashed arrows are theoretical predictions from refs 7 and 19. The dotted black arrow represents the experimental dangling frequency in $X^-\cdot(D_2O)$ from ref 19. Bottom panel: same as the top panel for the OOP frequency (see text). All frequencies are expressed relative to the corresponding average symmetric and asymmetric stretches of the isolated H_2O (ω^-_{RMPD} = 3770 cm^{-1}; ω^-_{exp} = 3707 cm^{-1}) .

frequencies of the IR spectrum of the dimer. The plots were extracted from the Fourier transform of the second derivative of the dipole autocorrelation function of the water molecule,[33] namely:

$$I(\omega) \propto \int_0^\infty dt\, \cos(\omega t)\langle \dot{\mu}(t)\cdot\dot{\mu}(0)\rangle_{RPMD} \qquad (9)$$

where $\langle\cdots\rangle_{RPMD}$ denotes a RPMD average.[40] To eliminate spurious signals originating from the fast modes of the intrapolymer interactions, the time correlation functions were evaluated following the procedure described in ref 41. This methodology consists of performing RPMD simulations while applying a Langevin thermostat coupled only to the internal modes of the ring polymer.

The top panel of Figure 3 contains results for the stretching band. The solid-line plot corresponds to results from a 10 ns trajectory that included several H−D interchange episodes between dangling and connective positions. The overall line shape can be viewed as containing two bands at $\omega_{rel} \sim 0$ and -1200 cm^{-1}, which clearly correspond to localized OH and OD stretching motions, respectively. In each band, two subbands are also clearly perceptible and can be ascribed to

DOI: 10.1021/acs.jpcb.5b05561
J. Phys. Chem. B XXXX, XXX, XXX−XXX

stretching motions involving H_c and H_d or D_c and D_d atoms. Such correspondence is very clearly manifested if one splits the full time correlation function of eq 9 into contributions from those time intervals during which the connectivity patterns are preserved: the dashed (dotted) line corresponds to the spectrum obtained from correlation functions collected during time intervals with $I^-\cdot(H_cOD_d)$ ($(I^-\cdot(D_cOH_d))$ connectivity.

The comparison between the calculated relative frequencies and the experimental results is also instructive. Except for the position of the connective-H peak, which falls ~30 cm^{-1} higher than the experimental value, the three other calculated signals agree well and are comparable to results obtained from high-quality quantum calculations reported in refs 7 and 19. The one frequency mismatch is akin to that already reported by us for OH stretching motions along water−water hydrogen bonds in single-donor water molecules exhibiting a second dangling H.[42]

In the lower panel of Figure 3, we display plots for the band arising from the OOP mode. Clearly, the larger red shift observed in the dotted line is associated with ionic binding to D. Moreover, because this mode is largely dominated by the displacement of the connecting atom,[18] a simple estimate of the difference in the shifts for the two isotopomers can be obtained as

$$\Delta(\omega_{rel}) = \omega_{rel}^{H_cOD_d} - \omega_{rel}^{H_dOD_c} \sim \frac{4}{\hbar}(\langle T_{H_c}^{OOP}\rangle - \langle T_{D_c}^{OOP}\rangle) = 103.7\ cm^{-1} \quad (10)$$

a value that agrees with the observed shift shown in Figure 3, $\Delta(\omega_{rel}) = 101\ cm^{-1}$.

III.B. The $I^-\cdot(H_2O)_{21}$ cluster. We will now move to the analysis of preferential isotopic solvation of anions in larger clusters. As a test case, we focused attention on the $I^-\cdot(H_2O)_{21}$ aggregate. Our goal is the characterization of the competition between water−water and ion−water interactions. This, in turn, might control the relative isotope stabilities at donor positions along these two different hydrogen bonds.

The choice of this "intermediate" cluster size was deliberate so as to avoid two scenarios in which one could anticipate that our approximate model is suspect. First, these are smaller aggregates for which our description is unlikely to reproduce the intricacies of the manifold of low-energy and stable conformers with well-defined symmetries that characterize small cluster structures with fewer than 10 water molecules.[7,13] These structures are controlled by subtleties originating from many-body effects that are absent in our present treatment. Second, the direct implementation of our force field in the analysis of larger, mesoscopic aggregates would be equally debatable because, again, it lacks an adequate treatment of many-body effects, which are believed to control ionic positions (inner versus surface) in cluster environments.[43−47]

Our starting point involved obtaining a series of initial conditions for $I^-\cdot(H_2O)_{21}$ clusters at $T = 50$ K by implementing a standard replica exchange scheme.[48−51] In doing so, we performed simulation runs for a set of 15 noninteracting replica cluster systems, simulated classically for about 10 ns and thermalized at temperatures in the interval between 50 and 250 K. At regular intervals of the order of 10 ps, swap-trial moves of configurations from trajectories at neighboring temperatures were attempted, with acceptance criteria controlled by a Metropolis algorithm.[52] After proper equilibration, 10 statistically independent configurations from the lowest temperature were used as initial conditions for quantum RPMD canonical ensemble runs. In Figure 1c we present a snapshot of one representative configuration; it can be roughly portrayed in terms of an aqueous domain of irregular shape, hosting the ionic solute in a nested structure. In this cluster size regime, there is no clear distinction between bulklike hydration and surface states. Typically, the solute-first solvation shell looks incomplete and is composed of $n = 6-7$ water molecules acting as double donors of HB to the I^- and to a neighboring water molecule lying at the outer (second) solvation shell. From the dynamical side, in this thermal regime, the clusters exhibit solidlike characteristics with practically no diffusive motions.

Armed with these initial configurations, we examined simultaneous H-to-D exchanges in the set of n tagged molecules, namely:

$$I^-\cdot(D_cOH_w)_n \rightarrow I^-\cdot(H_cOD_w)_n \quad (11)$$

where, in eq 11, the subscript "w" indicates an atom acting as HB donor to a water molecule in the second solvation shell (see Figure 1c). The free energy associated with the previous transformation can be estimated in a straightforward fashion using standard thermodynamic integration techniques,[53] namely:

$$\Delta A = \int_0^1 \left\langle \frac{\partial A(\lambda)}{\partial \lambda} \right\rangle_\lambda d\lambda \quad (12)$$

where the control parameter λ determines the reversible transformation of the mass in each one of the n water molecules, and $\langle\cdots\rangle_\lambda$ denotes a canonical ensemble average taken with the masses fixed at $\{m_i(\lambda)\}$. Reversible transformations were carried out following a procedure similar to one described in ref 17, where we refer the reader for additional details.

Figure 4 contains results for cumulative integrals of the type

$$\Delta A(\lambda) = \int_0^\lambda \left\langle \frac{\partial A(\lambda')}{\partial \lambda'} \right\rangle_{\lambda'} d\lambda' \quad (13)$$

The reversible transformation was performed along the following linear path, namely:

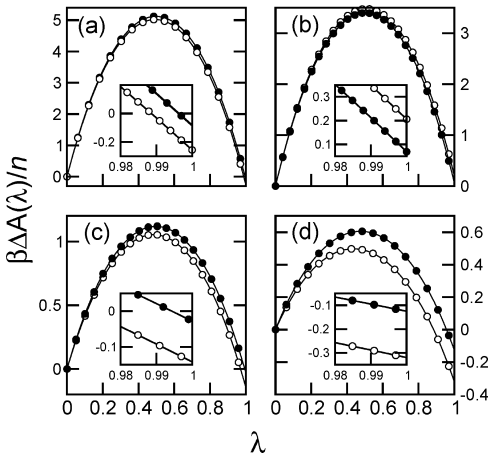

Figure 4. Cumulative integrals for the total and projected free-energy differences associated with the isotopic exchange shown in eq 11. (a) Total free energy, (b) parallel projection, (c) in-plane projection, and (d) out-of-plane projection. Open circles: $I^-\cdot(H_2O)_n$; black circles: $Br^-\cdot(H_2O)_n$. Insets show only areas near $\lambda = 1$.

DOI: 10.1021/acs.jpcb.5b05561
J. Phys. Chem. B XXXX, XXX, XXX−XXX

$$m_H(\lambda) = m_p(1 + \lambda)$$
$$m_D(\lambda) = m_p(2 - \lambda) \quad (14)$$

where m_p represents the proton mass. Panel a includes results for the total free-energy difference, whereas in panels (b) through (d) we present the corresponding projections. In all cases, the insets allow for a clearer view of the region close to the complete mass transformations, i.e., $\Delta A(\lambda = 1)$. The simultaneous analysis of the entries in Table 2b is instructive; note that the positive difference in $\langle T_{H_w} \rangle - \langle T_{H_c} \rangle$ anticipates the preference of the light isotope to lie at positions adjacent to the ionic solute. However, the magnitude of the latter difference is significantly smaller than the one we recorded for $\langle T_{H_d} \rangle - \langle T_{H_c} \rangle$ when we contrasted values for the connecting and dangling positions. This is to be expected because, in the present case, the comparison is established between donor atoms along alternative hydrogen bonds of comparable strengths, rather than with one that completely lacks an H-bond. The plot in the inset of panel (a) (open circles) confirms this tendency and shows a free-energy difference per hydrogen bond five times smaller, i.e., $\beta\Delta A/n \sim 0.25$. It is important to remark that the stabilization of light atoms at connecting positions to the ionic solute agrees with experimental evidence reported for aqueous solutions at ambient conditions[54−56] as well as recent theoretical predictions.[57]

The dissection of ΔA and the kinetic energy differences into projected contributions provides additional relevant information: (i) the contribution from the parallel projection is of opposite sign with respect to the other two and reveals that, along this direction, water−water hydrogen bonds look stronger and, correspondingly, the positional dispersion should be larger than that in which the I^- acts as acceptor; and (ii) the OOP dynamical mode still controls the global stabilization of light isotopes at I^-···HO hydrogen bonds.

An additional feature that confirms the previous trend is presented in Figure 5. The upper plots correspond to RPMD OH stretching bands along these two different hydrogen bonds. To extract clear signals, in Figure 5 we show results from simulations in which all hydrogens were transformed into D except the tagged ones contributing to the localized dynamical mode of interest. Note that the O···HO peak (solid line) appears to be ∼50 cm^{-1} red-shifted with respect to the I^-···HO one (dashed line). Interestingly, the latter displacement is akin to those reported by Kropman et al.[58] for the OH stretch vibration and the X^-···HO in solution. In passing, we stress that the latter tendency is at odds with experimental results reported for small clusters, such as, for example, the $I^-\cdot(H_2O)_2$ trimer. There, the signals from OH stretching along the ionic HBs present larger red shifts than those localized along interwater HBs.[2] As such, we are led to conclude that the presence of growing numbers of nearby water molecules induces stronger water−water interactions at the expense of weakening ionic bonds, most probably as a result of energetic competition.

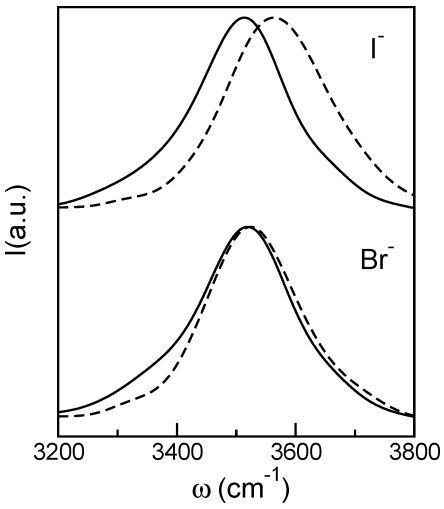

Figure 5. RPMD absorption spectra for $X^-\cdot(H_2O)_{21}$ clusters at T = 50 K (X = I or Br). The plots are restricted to OH stretching signals from water molecules lying in the solute first solvation shell. Solid lines: O··· HO hydrogen bond connectivity; dashed lines: X^-···HO hydrogen bond connectivity. To facilitate the comparison, the line shapes were normalized to equal maximum intensities.

Before closing our analysis, we will briefly comment on the isotopic stabilization changes as we consider ionic solutes of smaller size. In Table 1 and Figure 3, we also present RPMD results for geometrical parameters of the global minimum and the frequencies shifts in the IR spectrum of the $Br^-\cdot(H_2O)$ dimer. The quality of the agreement with experimental results and quantum calculations remains comparable to the one observed for the $I^-\cdot(H_2O)$ case. The plots in Figure 4 (black circles) show that, in the $Br^-\cdot(H_2O)_{21}$ aggregate, the global H-stabilization free energy and the corresponding projections drop by a factor of ∼2−3 compared to the $I^-\cdot(H_2O)_{21}$ results. At the same time, the shift in the RPMD signals displayed in the lower part of Figure 5 is reduced to ∼15 cm^{-1} but remains comparable to the experimental result.[58] The physical interpretation of these trends is straightforward, considering the stronger character of the ionic Br^-···HO HB, whose strength becomes closer to the one prevailing along interwater bonding. As such, the stabilization of light atoms adjacent to anionic solutes of smaller sizes should progressively diminish, a trend which accords with results obtained from electrochemical cell measurements[54] and D/H fractionation in gas and solution phases.[56]

IV. CONCLUDING REMARKS

The quantum simulation results presented in this paper provide microscopic insights into the preferential solvation of H and D isotopic species in the closest solvation shells of anionic species dissolved in water nanoclusters. For the particular case of the $I^-\cdot(HOD)$ dimer, our thermodynamic analysis shows a clear propensity of the light isotope to lie at dangling positions. From a qualitative perspective, at temperatures close to ∼50 K, our simulations predict a 3:1 proportion between the equilibrium populations of $I^-\cdot(DOH)$ isomers and that of its $I^-\cdot(HOD)$ isotopomer. Looking for the origins of such stabilization, we analyzed different projections of the nuclear kinetic energies of the different atoms, which closely reflect their corresponding local spatial extents. In particular, we found that the relative stabilization is controlled by the quantum dispersions along directions perpendicular to the plane of the water molecule. From a dynamical perspective, these directions have been previously identified with normal mode coordinates corresponding to low-frequency, out-of-plane bend motions[18] that, invoking a simple ZPE analysis, would drive the observed stabilization. Despite the simplicity of the implemented force field, the quality of the present predictions for the relative frequencies observed in the infrared spectrum of the dimer is

DOI: 10.1021/acs.jpcb.5b05561
J. Phys. Chem. B XXXX, XXX, XXX−XXX

quite satisfactory and, in most cases, comparable to those reported from high quality quantum calculations at 0 K.

We extended our analysis to larger clusters of the type $I^-\cdot(H_2O)_{21}$ to examine possible modifications of the previous scenario derived from the presence of an increasing number of solvent molecules. In this case, we gauged the competitive characteristics between isotopic stabilizations at donor positions in ion−water hydrogen bonds versus water−water ones, the latter linking the first solvation shell with the adjacent, second shell. We stress that, in this cluster size regime, the solvation of these anions consistently takes the form of an irregular cluster, such that one cannot establish a clear difference between bulklike (i.e., fully solvated) and surface (i.e. partially solvated) ionic configurations. For the purposes of the present study, this distinction does not play a key role because the hydrogen atoms are, in any case, engaged in an interaction with either the ion or another water molecule. The key element controlling the relative isotopic stability is the difference between the quantum kinetic energies of H atoms at these different connective positions.

Contrasting with the dimer case, our results predict a preferential connectivity of the type $I^-\cdots$HOD in contraposition to the $I^-\cdots$DOH alternative, although from a quantitative point of view, the magnitude of the resulting stabilization is five times smaller than the one registered in the dimer case. Still, in these larger clusters, the key feature driving the H propensity is the differences in the quantum OOP spatial extent. Finally, our study included a brief exploratory analysis performed along $Br^-\cdots$HO hydrogen bonds showed an additional drop in the H stabilization by a factor of ∼2−3, a result that agrees with experimental tendencies reported in bulk aqueous phases at ambient conditions.[54,56,58]

In the present context, several open questions remain and will certainly deserve additional investigation. Of these, two are particularly relevant; the first concerns how isotopic preference would evolve in the solvation shells of smaller anions, such as F^-, where the role of intermolecular proton transfer should necessarily introduce nontrivial modifications in the simplified picture presented here. However, the explicit incorporation of electronic polarization in the anionic species should also modulate the delicate interplay between ion−water and water−water interactions that, in turn, might control major structural differences, e.g., the presence of surface or inner solvation states. This introduces more complexities in the thermodynamic analysis of the isotopic stabilization in larger aggregates along different intramolecular connectivity patterns that, in addition to the aforementioned ion−water and water−water hydrogen bondings, should also include the hypothetical presence of dangling states at surface solvation states. In all cases, before attempting an answer, there is a clear need for more refined force fields.

AUTHOR INFORMATION

Corresponding Author

*E-mail: dhlaria@cnea.gov.ar.

Notes

The authors declare no competing financial interest.

ACKNOWLEDGMENTS

D.L. is a staff member of CONICET Argentina. P.J.R. acknowledges the support of the U.S. National Science Foundation (CHE-1362381).

REFERENCES

(1) Robertson, W. H.; Johnson, M. A. Molecular Aspects of Halide Ion Hydration: The Cluster Approach. *Annu. Rev. Phys. Chem.* **2003**, *54*, 173−213.

(2) Ayotte, P.; Nielsen, S. B.; Weddle, G. H.; Johnson, M. A.; Xantheas, S. S. Spectroscopic Observation of Ion-Induced Water Dimer Dissociation in the $X^-\cdot(H_2O)_2$ (X= F, Cl, Br, I) Clusters. *J. Phys. Chem. A* **1999**, *103*, 10665−10669.

(3) Ayotte, P.; Weddle, G. H.; Kim, J.; Johnson, M. A. Mass-Selected Matrix Isolation Infrared Spectroscopy of the $I^-\cdot(H_2O)_2$ Complex: Making and Breaking the Inter-Water Hydrogen-Bond. *Chem. Phys.* **1998**, *239*, 485−491.

(4) Roscioli, J. R.; Diken, E. G.; Johnson, M. A.; Horvath, S.; McCoy, A. B. Prying Apart a Water Molecule with Anion H-Bonding: A Comparative Spectroscopic Study of the $X^-\cdot H_2O$ (X = OH, O, F, Cl, and Br) Binary Complexes in the 600−3800 cm^{-1} Region. *J. Phys. Chem. A* **2006**, *110*, 4943−4952.

(5) Sung, S. S.; Jordan, P. C. Structures and Energetics of Monovalents Ion-Water Microclusters. *J. Chem. Phys.* **1986**, *85*, 4045−4051.

(6) Lin, S.; Jordan, P. C. Structures and Energetics of Monovalents Ion-Water Microclusters: II. Thermal Phenomena. *J. Chem. Phys.* **1988**, *89*, 7492−7501.

(7) Lee, H. M.; Kim, J. S. Structures and Spectra of Iodide-Water Clusters $I^-(H_2O)_{n=1,6}$: An ab-initio Study. *J. Chem. Phys.* **2001**, *114*, 4461−4471.

(8) Perera, L.; Berkowitz, M. L. Stabilization Energies of Cl^-, Br^-, and I^- Ions in Water Clusters. *J. Chem. Phys.* **1993**, *99*, 4222−4224.

(9) Combariza, J. W.; Kestner, N. R.; Jortner, J. Energy-Structure Relationships for Microscopic Solvation of Anions in Water Clusters. *J. Chem. Phys.* **1994**, *100*, 2851−2864.

(10) Perera, L.; Berkowitz, M. L. Structures of $Cl^-(H_2O)_n$ and $F^-(H_2O)_n$ (n = 2,3,...,15) Clusters. Molecular Dynamics Computer Simulations. *J. Chem. Phys.* **1994**, *100*, 3085−3093.

(11) Xantheas, S. S. Quantitative Description of Hydrogen Bonding in Chloride-Water Clusters. *J. Phys. Chem.* **1996**, *100*, 9703−9713.

(12) Baik, J.; Kim, J.; Majumdar, D.; Kim, K. S. Structures, Energetics, and Spectra of Fluoride-Water Clusters $F^-(H_2O)_n$, n = 1−6: Ab Initio Study. *J. Chem. Phys.* **1999**, *110*, 9116−9127.

(13) Kim, J.; Lee, H. M.; Suh, S. B.; Majumdar, D.; Kim, K. S. Comparative *ab-initio* Study of the Structures, Energetics and Spectra of $X^-\cdot(H_2O)_{n=1-4}$ [X = F, Cl, Br, I] Clusters. *J. Chem. Phys.* **2000**, *113*, 5259−5272.

(14) Thompson, W. H.; Hynes, J. T. Frequency Shifts in the Hydrogen-Bonded OH Stretch in Halide-Water Clusters. The Importance of Charge Transfer. *J. Am. Chem. Soc.* **2000**, *122*, 6278−6286.

(15) McCunn, L. R.; Roscioli, J. R.; Johnson, M. A.; McCoy, A. B. An H/D Isotopic Substituion Study of the $H_5O_2^+\cdot Ar$ Vibrational Predissociation Spectra: Exploring the Putative Role of Fermi Resosnces in the Bridging Proton Fundamentals. *J. Phys. Chem. B* **2008**, *112*, 321−327.

(16) Vendrell, O.; Gatti, F.; Meyer, H.-D. Full Dimensional (15 Dimensional) Quantum-Dynamical Simulation of the Protonated Water-Dimer IV: Isotope Effects in the Infrared Spectra of $D(D_2O)_2$, $H(D_2O)_2$ and $D(H_2O)_2$ Isotopologues. *J. Chem. Phys.* **2009**, *131*, 034308.

(17) Videla, P. E.; Rossky, P. J.; Laria, D. Surface Isotope Segregation as a Proble of Temperature in Water Nanoclusters. *J. Phys. Chem. Lett.* **2014**, *5*, 2375−2379.

(18) Diken, E. G.; Shin, J.-W.; Price, E. A.; Johnson, M. A. Isotopic Fractionation and Zero-Point Effects in Anionic H-Bonded Complexes: a Comparison of the $I^-\cdot$HDO and $F^-\cdot$HDO Ion−Molecule Clusters. *Chem. Phys. Lett.* **2004**, *387*, 17−22.

(19) Horvath, S.; McCoy, A. B.; Elliott, B. M.; Weddle, G. H.; Roscioli, J. R.; Johnson, M. A. Anharmonicities and Isotopic Effects in the Vibrational Spectra of $X^-\cdot H_2O$, $\cdot$HDO, and $\cdot D_2O$ [X = Cl, Br, and I] Binary Complexes. *J. Phys. Chem. A* **2010**, *114*, 1556−1568.

DOI: 10.1021/acs.jpcb.5b05561
J. Phys. Chem. B XXXX, XXX, XXX−XXX

(20) Rheinecker, J. L.; Bowman, J. M. The Calculated Infrared Spectrum of Cl^-H_2O Using a Full Dimensional ab-initio Potential Surface and Dipole Moment Surface. *J. Chem. Phys.* **2006**, *124*, 131102.
(21) Irle, S.; Bowman, J. Direct Ab Initio Variational Calculation of Vibrational Energies of the $H_2O\cdots Cl^-$ Complex and Resolution of Experimental Differences. *J. Chem. Phys.* **2000**, *113*, 8401−8403.
(22) Huang, X.; Habershon, S.; Bowman, J. M. Comparison of Quantum, Classical, and Ring-Polymer Molecular Dynamics Ion-Water Microclusters: II. Thermal Phenomena. *Chem. Phys. Lett.* **2008**, *450*, 253−257.
(23) Habershon, S.; Manolopoulos, D. E.; Markland, T. E.; Miller, T. F., III Ring-Polymer Molecular Dynamics: Quantum Effects in Chemical Dynamics from Classical Trajectories in an Extended Phase Space. *Annu. Rev. Phys. Chem.* **2013**, *64*, 387.
(24) See, for example, Tuckerman, M. E. Chapter 10. *Statistical Mechanics: Theory and Molecular Simulation*; Oxford University Press: Oxford, 2010.
(25) Habershon, S.; Markland, T. E.; Manolopoulos, D. E. Competing Quantum Effects in the Dynamics of a Flexible Water Model. *J. Chem. Phys.* **2009**, *131*, 024501.
(26) Markland, T. E.; Berne, B. J. Unraveling Quantum Mechanical Effects in Water Using Isotopic Fractionation. *Proc. Natl. Acad. Sci. U. S. A.* **2012**, *109*, 7988−7991.
(27) Joung, S.; Cheatham, T. E., III Determination of Alkali and Halide Monovalent Ion Parameters for Use in Explicitly Solvated Biomolecular Simulations. *J. Phys. Chem. B* **2008**, *112*, 9020−9041.
(28) Jensen, K. P.; Jorgensen, W. L. Halide, Ammonium, and Alkali Metal Ion Parameters for Modeling Aqueous Solutions. *J. Chem. Theory Comput.* **2006**, *2*, 1499−1509.
(29) Peng, T.; Chang, T.; Sun, X.; Nguyen, A. V.; Dang, L. X. Development of Ions-TIP4P-Ew Force Fields for Molecular Processes in Bulk and at the Aqueous Interface Using Molecular Simulations. *J. Mol. Liq.* **2012**, *173*, 47−54.
(30) Lamoureux, G.; Roux, B. Absolute Hydration Free Energy Scale for Alkali and Halide Ions Established from Simulations with a Polarizable Force Field. *J. Phys. Chem. B* **2006**, *110*, 3308−3322.
(31) Yu, H.; Whitfield, T. W.; Harder, E.; Lamoureux, G.; Vorobyov, I.; Anisimov, V. M.; MacKerell, A. D., Jr.; Roux, B. Simulating Monovalent and Divalent Ions in Aqueous Solution Using a Drude Polarizable Force Field. *J. Chem. Theory Comput.* **2010**, *6*, 774−786.
(32) Karmakar, A.; Chandra, A. Water in Hydration Shell of an Iodide Ion: Structure and Dynamics of Solute-Water Hydrogen Bonds and Vibrational Spectral Diffusion from First-Principles Simulations. *J. Phys. Chem. B* **2015**, *119*, 8561−8572.
(33) Habershon, S.; Fanourgakis, G. S.; Manolopoulos, D. E. Comparison of Path Integral Molecular Dynamics Methods for the Infrared Absorption Spectrum of Liquid Water. *J. Chem. Phys.* **2008**, *129*, 74501.
(34) Tuckerman, M.; Berne, B. J.; Martyna, G. J. Reversible Multiple Time Scale Molecular Dynamics. *J. Chem. Phys.* **1992**, *97*, 1990−2001.
(35) Martyna, G. J.; Tuckerman, M. E.; Tobias, D. J.; Klein, M. L. Explicit Reversible Integrators for Extended Systems Dynamics. *Mol. Phys.* **1996**, *87*, 1117−1157.
(36) Frenkel, D.; Smit, B. Chapter 7. *Understanding Molecular Simulation From Algorithms to Applications*; Academic Press: London, 2001.
(37) Ceriotti, M.; Markland, D. E. Efficient Methods and Practical Guidelines for Simulating Isotope Effects. *J. Chem. Phys.* **2013**, *138*, 14112.
(38) Herman, M. F.; Bruskin, J.; Berne, B. J. On Path Integral Monte Carlo Simulations. *J. Chem. Phys.* **1982**, *76*, 5150−5155.
(39) Liu, J.; Andino, R. S.; Miller, C. M.; Chen, X.; Wilkins, D. M.; Ceriotti, M.; Manolopoulos, D. E. A Surface-Specific Isotope Effect in Mixtures of Light and Heavy Water. *J. Phys. Chem. C* **2013**, *117*, 2944−2951.
(40) Craig, I. R.; Manolopoulos, D. E. Quantum Statistics and Classical Mechanics: Real Time Correlation Functions from Ring Polymer Molecular Dynamics. *J. Chem. Phys.* **2004**, *121*, 3368−3373.
(41) Rossi, M.; Ceriotti, M.; Manolopoulos, D. E. How to Remove the Spurious Resonances from Ring Polymer Dynamics. *J. Chem. Phys.* **2014**, *140*, 234116.
(42) Videla, P. E.; Rossky, P. J.; Laria, D. Nuclear Quantum Effects on the Structure and the Dynamics of [H2O]8 at Low Temperatures. *J. Chem. Phys.* **2013**, *139*, 174315.
(43) Tobias, D. J.; Jungwirth, P.; Parrinello, M. Surface Solvation of Halogen Anions in Water Clusters: An Ab Initio Molecular Dynamics Study of the $Cl\text{-}(H_2O)_6$ Complex Clusters. The Importance of Charge Transfer. *J. Chem. Phys.* **2001**, *114*, 7036−7044.
(44) Jungwirth, P.; Tobias, D. J. Ions at the Air/Water Interface. *J. Phys. Chem. B* **2002**, *106*, 6361−6373.
(45) Jungwirth, P.; Tobias, D. J. Chloride Anion on Aqueous Clusters, at the Air-Water Interface, and in Liquid Water: Solvent Effects on Cl^- Polarizability. *J. Phys. Chem. A* **2002**, *106*, 379−383.
(46) Yoo, S.; Lei, Y. A.; Zeng, X. C. Effect of Polarizability of Halide Anions on the Ionic Solvation in Water Clusters. *J. Chem. Phys.* **2003**, *119*, 6083−6091.
(47) Caleman, C.; Hub, J. S.; van Maaren, P. J.; van der Spoel, D. Atomistic Simulation of Ion Solvation in Water Explains Surface Preference of Halides. *Proc. Natl. Acad. Sci. U. S. A.* **2011**, *108*, 6838−6842.
(48) Sugita, Y.; Okamoto, Y. Replica-Exchange Molecular Dynamics Method for Protein Folding. *Chem. Phys. Lett.* **1999**, *314*, 141−151.
(49) Zhang, W.; Wu, C.; Duan, Y. Convergence of Replica Exchange Molecular Dynamics. *J. Chem. Phys.* **2005**, *123*, 154105.
(50) Earl, D. J.; Deem, M. W. Parallel Tempering: Theory, Applications, and New Perspectives. *Phys. Chem. Chem. Phys.* **2005**, *7*, 3910−3916.
(51) Kone, A.; Kofke, D. A. Selection of Temperature Intervals for Parallel-Tempering Simulations. *J. Chem. Phys.* **2005**, *122*, 206101.
(52) Metropolis, N.; Rosenbluth, A. W.; Rosenbluth, M. N.; Teller, A. H.; Teller, E. Equation of State Calculations by Fast Computing Machines. *J. Chem. Phys.* **1953**, *21*, 1087−1092.
(53) Vanicek, J.; Miller, W. H. Efficient Estimators for Quantum Instanton Evaluation of the Kinetic Isotope Effects: Application to the Intramolecular Hydrogen Transfer in Pentadiene. *J. Chem. Phys.* **2007**, *127*, 114309.
(54) Greyson, J. The Influence of the Alkali Halides on the Structure of Water. *J. Phys. Chem.* **1967**, *71*, 2210−2213.
(55) Kakiuchi, M. Temperature Dependence of Frationation of Hydrogen Isotopes in Aqueous Sodium Chloride Solutions. *J. Solution Chem.* **1994**, *23*, 1073−1087.
(56) Kakiuchi, M. Hydrogen Isotope Fractionation in Aqueous Halide Solutions. *Z. Naturforsch., A: Phys. Sci.* **1997**, *52*, 811−820.
(57) Oi, T.; Morimoto, H. Oxygen and Hydrogen Isotopic Preference in Hydration Spheres of Chloride and Sulfate Ions. *Z. Phys. Chem.* **2013**, *227*, 807−819.
(58) Kropman, M. F.; Bakker, H. J. Vibrational Relaxation of Liquid Water in Ionic Solvation Shells. *Chem. Phys. Lett.* **2003**, *370*, 741−746.

DOI: 10.1021/acs.jpcb.5b05561
J. Phys. Chem. B XXXX, XXX, XXX−XXX